

Donor activation and electronic screening at an antimony δ layer in silicon

J. M. C. Thornton and R. J. Cole

*Interdisciplinary Research Centre in Surface Science and Department of Physics, University of Liverpool,
P.O. Box 147, L69 3BX, United Kingdom*

D. J. Gravesteijn

Philips Research Laboratories, 5600 JA Eindhoven, The Netherlands

P. Weightman

*Interdisciplinary Research Centre in Surface Science and Department of Physics, University of Liverpool,
P.O. Box 147, L69 3BX, United Kingdom*

(Received 22 February 1996; revised manuscript received 7 May 1996)

Electron spectroscopic studies of highly concentrated δ layers of Sb impurity atoms in epitaxially grown Si(001) have revealed the presence of two main Sb environments. An analysis of the kinetic energies of the core-level photoemission and Auger spectra of Sb in terms of the Auger parameter shows that the core holes on each site are less well screened than in the pure element. A simultaneous analysis of shifts in the initial-state and final-state Auger parameters of the two sites and bulk Sb enables one site to be identified with positively charged donors, and the other with neutral Sb, possibly in clusters, defects, or interstitial sites. The donors are found to contribute between 0.12 and 0.20 electrons per Sb atom, in agreement with transport measurements on similarly prepared specimens. The on-site screening of core holes on the two sites, dq/dN , is found to be 0.82 and 0.93 for the δ_1 and δ_2 sites, respectively. This result is consistent with the expectation that the donor site will be better screened by access to the electron gas of donated electrons. [S0163-1829(96)05936-X]

INTRODUCTION

One of the current major themes of semiconductor research is the creation of high doping levels with sharp spatial profiles for use in high-speed devices such as heterojunction bipolar transistors. The demand for these kinds of structures, however, seems to be almost offset by the technical difficulties experienced in their fabrication. The problems are particularly hard to overcome for n -type dopants in silicon, where strong surface segregation and a low incorporation probability¹ during growth severely limit the doping profile attainable. Antimony is one of the n -type dopants which has been widely used in high concentration and δ -doping studies,²⁻⁵ which, although it segregates strongly and is therefore hard to control, does have the practical advantage of being easy to evaporate from a Knudsen cell.

A number of different approaches have been made to the problem of creating highly concentrated δ layers of Sb in Si, such as ion implantation of Sb, or low-temperature epitaxial growth of the Si.⁵ These and other approaches to the creation of δ layers have various advantages and difficulties, with perhaps the best understood so far being that of solid phase epitaxy (SPE).^{4,6} In this technique, a complete, or near to complete, monolayer of Sb is deposited onto an epitaxially prepared Si substrate surface followed by a layer of Si at low temperature. The Si is amorphous at the temperatures used, though the overlayer can be recrystallized by annealing, with only very limited diffusion of the Sb away from the original position of the layer. The main advantage this particular preparation method offers is that it yields complete incorporation of the Sb in the Si, though this does not extend to the electrical activity of the dopant atoms. In order to be electri-

cally active, the Sb dopant atoms require either a pregrowth or postgrowth annealing stage.^{7,8} Complete incorporation is an important factor in the experiments to be described here, which are surface sensitive, and so might be confused by the existence of both surface and buried environments of Sb. For this reason we have concentrated our studies on SPE-grown samples, and have investigated the local chemical and electronic environment of the Sb dopant atoms, with particular attention paid to charge transfer and local screening effects. To our knowledge this is the first direct measurement of local charge and screening on dopant atoms, as opposed to inference through electrical measurements.

In this work, we describe an approach to the determination of the activation level, local charge, and local screening on Sb impurities in a δ layer in Si(001). The approach is based on the measurement by electron spectroscopy of the dependence of the Auger parameter on the local environment. We analyze the results in terms of a local potential model which has previously been shown to be a good description of ground-state charge transfer and local screening in a number of systems.⁹⁻¹⁴ We find that a monolayer of Sb in Si occupies two environments with the same depth distribution, which we attribute to electrically active and inactive sites. We are able to quantify the extent of on-site screening of core holes on the two sites, and determine the local charge on the activated impurities.

EXPERIMENT

Sb-doped δ layers were grown on (001) oriented 4-in.-diameter Si substrates of p -type 1000- Ω cm float-zone material. Following the thermal desorption of the native oxide, a

buffer layer of Si was grown epitaxially at a temperature of 685 °C to a thickness of 1500 Å. Details of the molecular-beam epitaxy (MBE) apparatus and technique have been published elsewhere.¹⁵ A layer of Sb was then deposited from a Knudsen cell onto this prepared surface to a concentration of $3.5 \times 10^{14} \text{ cm}^{-2}$, as measured subsequently using Rutherford backscattering spectrometry (RBS). After cooling to room temperature, amorphous Si layers of 25- and 45 Å thicknesses were deposited over the Sb. The top layers were then recrystallized by ramping the temperature up to 560 °C and cooling back to room temperature. No extra annealing time was needed due to the very small thicknesses of the Si overlayers, which were chosen to permit electron spectroscopic techniques to be used to detect the Sb δ layer. On removal from the MBE chamber, the samples were etched in a 5% aqueous solution of HF to remove the surface oxide, and any surface Sb which may have been present.

The samples were transferred to an electron spectrometer,¹⁶ where the spectra from core-electron and Auger features were measured. These consisted of the Sb 3*d* and 4*d* core-level photoemission peaks, and the Sb $M_{4,5}N_{4,5}N_{4,5}$ Auger transitions. These could all be excited by Al $K\alpha$ radiation, which was monochromated to a linewidth of 0.4 eV. The hemispherical electron analyzer was used in a fixed transmission mode, giving a resolution of 0.07 eV for the Auger features. Spectra were obtained at both normal emission, and at an angle of 50° between the sample normal and the electron emission in order to investigate the surface species and depth distribution of the Sb.

The samples were also investigated using higher-energy synchrotron radiation ($h\nu=4500 \text{ eV}$) to excite the Sb $L_{2,3}M_{4,5}N_{4,5}$ transitions. This was performed on beamline IRC-4.2 at Daresbury Laboratory, U.K. The Auger electrons were collected with a similar analyzer to the in-house spectrometer, though in this case the sensitivity was enhanced by operating at a reduced resolution, corresponding to a Gaussian broadening of 0.6 eV.

Core-level x-ray photoemission spectroscopy (XPS) and $M_{4,5}N_{4,5}N_{4,5}$ Auger transitions of bulk Sb were also measured from polycrystalline material grown by depositing Sb onto a room-temperature GaAs substrate using a Knudsen cell operating at 520 °C. After a 30-min deposition, no photoemission from the substrate could be seen, indicating that the thickness of the polycrystalline Sb overlayer was in excess of 150 Å.

RESULTS

Core levels

The Sb 4*d* and 3*d*_{3/2} core levels obtained from the sample grown with a 25-Å Si top layer are shown by the dots in Figs. 1(a) and 1(b), and are representative of both of the specimens, though as expected the Sb features showed a reduction in absolute intensity when measured for the specimen with the 45-Å top layer of Si. The spectra shown in Figs. 1(a) and 1(b) were collected at normal emission.

The Sb 3*d*_{3/2} peak is shown in Fig. 1(b) rather than the more intense 3*d*_{5/2}, due to the proximity of the latter to the O 1*s* core-level photoemission line, which occurs in the spectral region between the two Sb spin-orbit-split components. Fortunately, the Sb 3*d* spin-orbit-split components are sepa-

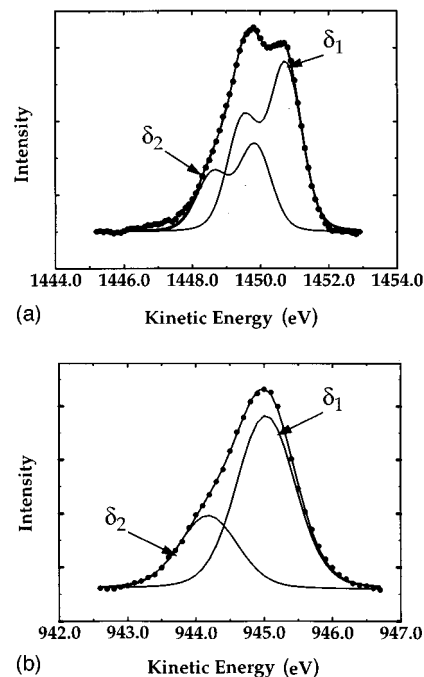


FIG. 1. (a) A normal-emission XPS spectrum of the Sb 4*d* core level from a δ layer, buried by 25 Å in Si(001). The spectrum is shown fitted with two components separated by 0.85 eV in energy (δ_1 and δ_2), which are believed to be neutral precipitate and substitutional donors, respectively. (b) An XPS spectrum of the Sb 3*d*_{3/2} core level under the same conditions as in (a).

rated in energy by approximately 9 eV, so the 3*d*_{3/2} is not affected significantly by the O 1*s* emission. The fact that the Sb 4*d* spectrum does not have the form of a single spin-orbit doublet makes it immediately clear that Sb is present in more than one environment. An analysis of the peak shapes using a curve-fitting routine established that both 3*d* and 4*d* core levels consist of two components; one large peak (labeled δ_1), and a smaller one (δ_2) 0.85 eV to higher binding energy. The spectral profiles of both Sb core levels can be attributed to an envelope of two identically shaped contributions, 0.85 eV apart, and with a relative intensity ratio of 1.9:1 ($\delta_1:\delta_2$). The parameters used in the fitting are shown in Table I, and the fits themselves are shown by the lines in Figs. 1(a) and 1(b). A number of different approaches were made to analyze the data, including more than two components in the line shape, though the best fit was found to be for two components of identical form. It might be possible to interpret the Sb 3*d*_{3/2} core-level line shape in terms of a single, highly asymmetric component. Such an interpretation would not be consistent with the 4*d* line shape, however, and it would be difficult to account for such a large asymmetry in terms of the usual Doniach-Sunjić mechanism,¹⁷ given that the line shape observed from metallic Sb is symmetrical. We can also eliminate the possibility that one of the Sb components arises from surface-oxidized Sb, since the angle-dependent studies showed no change in the relative intensity of the two components with takeoff angle.

The XPS results showed that the specimens had a thin silicon dioxide layer at the surface, and that the Sb was buried in the Si. It was found that the XPS line shape of the Sb core levels did not alter with emission angle, and did not

TABLE I. A table of the parameters used to obtain fits to the core-level photoemission peaks shown in Figs. 1(a) and 1(b).

XPS curve-fitting parameters	Sb 3d		Sb 4d	
	Sb 3d	Sb 4d	Sb 3d	Sb 4d
Lorentzian width	0.16 eV	0.18		
Gaussian width	0.90 eV	0.99 eV ^a		
Spin-orbit splitting	9 eV	1.25 eV		
Relative intensity of spin-orbit components	0.66	0.66		
Binding-energy difference ($\delta_2 - \delta_1$)	0.85 eV	0.87 eV		
Intensity ratio (δ_1/δ_2)	1.9	1.9		

^aThese Gaussian widths are broader than expected from the contribution arising from the resolution of the spectrometer (~ 0.4 eV). We attribute the extra width to inhomogeneous broadening arising from a statistical distribution of slightly different environments for each of the two sites, and local variation in band bending across the sample.

increase in intensity relative to the bulk Si 2*p* emission at grazing emission angles as found for the O 1*s* and Si 2*p* associated with SiO₂. This confirms the view that all the Sb remains buried in the Si top layer, and did not diffuse to the surface during growth, where it would have oxidized on removal of the specimen from the UHV growth apparatus. We note that the absence of any dependence of both the Sb 4*d* and 3*d*_{3/2} core-level line shapes on emission angle indicates that the environments giving rise to the δ_1 and δ_2 components have the same depth distribution. This view is further supported by the fact that although the 3*d* and 4*d* photoemission peaks occur at different kinetic energies, and hence different electron escape depths, the best fits to each spectrum yield the same $\delta_1:\delta_2$ intensity ratios (Table I). The experimental results for the binding energies of the Sb core levels for the Sb δ layer and bulk Sb are shown in Table II.

TABLE II. A table of the measured binding and kinetic energies of the Sb core-level and Auger electron features, where δ_1 and δ_2 are the two components identified by the fits to the core-level peaks. The final-state Auger parameter α is also given.

Binding and kinetic energies of Sb features in eV	Bulk Sb			
	Bulk Sb	δ_1	δ_2	δ
BE ^F 3 <i>d</i> _{3/2} ^a	539.1	538.4	539.2	
KE ^F <i>M</i> ₄ ^b	453.2			451.4
KE ^F <i>L</i> ₃ ^c	3023.7 (Ref.15)			3023.5
$\alpha = \text{KE}^F + \text{BE}$	992.3	989.8	990.6	

^aThese measured kinetic energies may be related to core-level binding energies referenced to the Fermi energy by the relationship: $\text{BE} = h\nu - \text{KE}^{\text{ANALYZER}} - \phi$, where the exciting photon energy was $h\nu = 1486.6$ eV, and the analyzer work function ϕ was 3.2 eV.

^bThe sharp peak associated with the ¹G₄ component is taken to represent the kinetic energy of the *M*₄*N*_{4,5}*N*_{4,5} Auger group. These results are referenced to the Fermi energy using $\text{KE}^F = \text{KE}^{\text{ANALYZER}} + \phi$, and are to within ± 0.2 eV.

^cThe kinetic energy corresponds to the maximum intensity of the *L*₃*M*_{4,5}*M*_{4,5} Auger group, which is dominated by the ¹G₄ component.

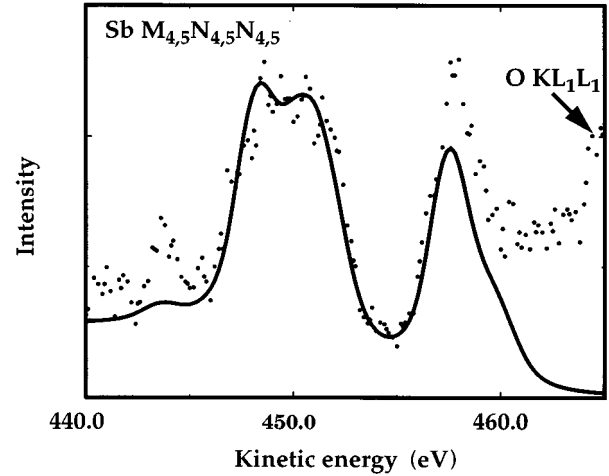


FIG. 2. The Sb *M*_{4,5}*N*_{4,5}*N*_{4,5} Auger transition obtained using Al *K* α radiation is shown by the dots, and is compared to a fit obtained by combining two *M*_{4,5}*N*_{4,5}*N*_{4,5} spectral profiles separated in kinetic energy by 0.8 eV, each of which has a spectral shape observed from bulk Sb. Only the *M*₅ group is shown, with a good fit due to the modification of the background by the O *KL*_{2,3}*L*_{2,3} Auger emission which is close in energy.

Auger features

The Sb *L*₃*M*_{4,5}*M*_{4,5} (~ 3000 eV) and *M*_{4,5}*N*_{4,5}*N*_{4,5} (~ 400 eV) groups of Auger features were measured using excitation from synchrotron radiation and a conventional laboratory x-ray source, respectively. For our purposes, measurement at the kinetic energies of the *M*_{4,5}*N*_{4,5}*N*_{4,5} Auger series are preferred due to the intrinsically narrower width of the spectral features and greater sensitivity of the electron analyzer used at these energies. From these samples, however, it proved to be difficult to measure the *M*_{4,5}*N*_{4,5}*N*_{4,5} group due to the close proximity in energy of the oxygen *KL*_{2,3}*L*_{2,3} Auger emission. This resulted in a high background emission which made it difficult to extract the small signal from the buried monolayer of Sb, and made analysis more difficult due to the altered shape of the background in the region of interest. The analysis was further complicated by the existence of extra spectral features in the region of interest when characteristic radiation from Mg and Al anodes were used, though this problem was overcome by the use of monochromated Al *K* α radiation, which, although it resulted in a significant reduction of intensity, did yield a greater signal to background intensity ratio. Despite these difficulties, it was possible to collect *M*_{4,5}*N*_{4,5}*N*_{4,5} spectra from the buried Sb layer due to the high sensitivity of the instrument used, and the data are shown in Fig. 2. Auger spectra were also obtained from a bulk polycrystalline Sb film, and the spectra were found to be in excellent agreement with the known atomic multiplet splittings and intensities for the components in the *M*_{4,5}*N*_{4,5}*N*_{4,5} Auger group.¹⁸

The experimental *M*_{4,5}*N*_{4,5}*N*_{4,5} spectrum from the Sb δ layer is shown by the dots in Fig. 2, and is compared to a simulated spectrum obtained by combining two *M*_{4,5}*N*_{4,5}*N*_{4,5} spectral profiles separated in kinetic energy by 0.8 eV each of which has the spectral shape observed from bulk Sb. It was found that a reasonable simulation of the observed width

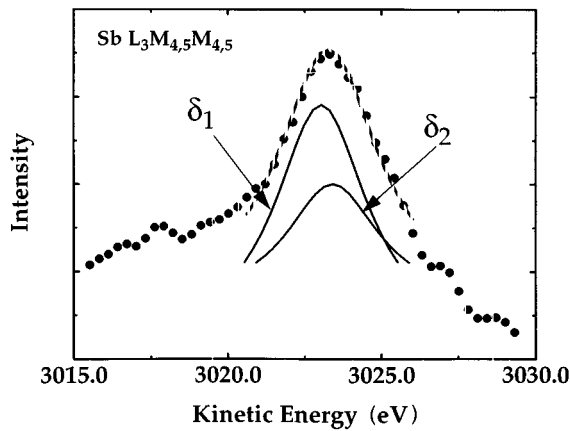


FIG. 3. The Sb $L_3M_{4.5}M_{4.5}$ Auger transition obtained using synchrotron radiation with an energy 4500 eV from the same buried δ layer of Sb as in Figs. 1 and 2. A fit to the $L_3M_{4.5}M_{4.5}; {}^1G_4$, showing the maximum acceptable shift between two components consisting of Lorentzian peaks (the FWHM is 2.8 eV), broadened with a 0.6-eV Gaussian instrumental contribution, is also shown overlaid. The components are offset in the vertical axis for clarity.

of the $M_5N_{4.5}N_{4.5}$ and $M_4N_{4.5}N_{4.5}$ groups could be obtained using any separation in energy of the two components from 0 to 0.8 eV, and a background of the Shirley form. It was not possible to reproduce both the M_4 and M_5 groups of the Auger spectrum simultaneously, since the spectra sit on a background which rises to higher kinetic energy and which arises from the O $KL_{2,3}L_{2,3}$ Auger emission. The figure shows a good simulation of the width of the M_5 group. An equivalent simulation of the M_4 group can also be obtained by correcting for the rising background. Regardless of the intensities or separations used in the simulations, the clear outcome is that the observed width of the $M_{4.5}N_{4.5}N_{4.5}$ groups limits any shift in energy between the two known environments to 0.8 eV or less. We define the difference in kinetic energy of the components from the two known environments as $\Delta E_k(\delta_2 - \delta_1)$.

The higher energy Sb $L_3M_{4.5}M_{4.5}; {}^1G_4$ Auger transition at approximately 3023 eV is shown in Fig. 3. This feature was difficult to obtain experimentally, and has a rather broad natural linewidth of ~ 3 eV.¹⁹ An analysis of this spectrum, however, has the advantage over the study of the $M_{4.5}N_{4.5}N_{4.5}$ spectra of being free from any spectral features arising from Si or its oxide. The full width at half maximum (FWHM) of this peak is 3.1 eV, which is smaller than that previously measured for bulk Sb (~ 4.0 eV).^{20,21} Our measurements were made using a higher-resolution setting for the electron analyzer than in the previous studies^{20,21} (~ 0.6 eV compared with ~ 2.0 eV), in the hope that we might resolve the spectra from the two environments identified in the core-level photoemission data. Models of the spectrum in terms of two components are dominated by the natural linewidth, though, from the narrowness of the Auger peak, it is clear that no large energy shift occurs between the components of the two known environments, in agreement with the analysis of the data for the Sb $M_{4.5}N_{4.5}N_{4.5}$ group in Fig. 2. This may be demonstrated by fitting the Auger peakshape with two Lorentzian peaks of 2.8-eV FWHM, and with a 2:1 intensity ratio, which are broadened with a Gaussian of 0.6

eV to account for the resolution of the electron analyzer. The data are easily fitted with a kinetic-energy shift of zero, and, regardless of relative energy, a kinetic-energy difference between the components greater than 0.4 eV gives an unacceptable representation of the data. A fit in the extreme case of a 0.4 eV energy difference is shown in Fig. 3 as a dashed line, together with the two components. We conclude from the analysis of the Sb $M_{4.5}N_{4.5}N_{4.5}$ and $L_3M_{4.5}M_{4.5}$ spectra that the data are consistent with the presence of two environments with a relative intensity of 2:1, and that the Auger splitting ΔE_k is ≤ 0.4 eV and possibly 0.0 eV. The experimental results for the kinetic energies are shown in Table II.

DISCUSSION

In seeking an explanation for the presence of two Sb sites, we note that the extremely high concentration of Sb at the δ layer is well above the maximum doping level achieved in this system,⁴ and that at higher annealing temperatures than those employed here, electron microscopy has revealed precipitation of Sb following this preparation.⁶ It is not clear, however, that clusters have formed in our specimens due to the relatively low temperature used in their preparation,²² though it remains a possibility. Any clusters would be expected to be small since there is no surface Sb, and the overlayer is only ~ 25 Å in thickness. It is possible that significant numbers of Sb atoms occupy interstitial positions and sites with imperfect coordination associated with vacancies and other defects. Electronically, the dopant concentration is so large that it easily exceeds the concentration necessary for the formation of an electron gas²³ which will screen the potential of the two-dimensional layer. In this circumstance we expect the donor levels to be smeared into the classical impurity band. The effective charge on donor sites will then depend on the position of the Fermi level relative to the states in the δ layer, and the degree of delocalization of the wave functions of the donor valence levels. The formation of an electron gas able to screen the δ layer as a whole leads us to expect that individual donor sites will experience near-metallic screening. It is difficult to draw any conclusions about the electronic structure of segregated or defect-associated Sb sites, except to observe that the small size of any clusters should significantly reduce local electron screening below that observed for pure Sb. The localized valence wave functions of electrically inactivated sites would also lead us to expect low electron screening. In the absence of a clear identity for the two environments that we observe, we attribute them to active and inactive sites, with no clear lead as to which is which.

The results of RBS measurements on these and similar samples show that between 50% and 80% of the Sb can be expected to be on substitutional sites, a result which does not enable unambiguous identification of either component of the XPS spectrum. The identification of two types of site is of course a simplified view of the real Sb environments which may exist under these conditions, as may be seen from the width of the Gaussian broadening contribution needed to fit the Sb core levels (Table I). This was between 0.9 and 1.0 eV for each site, and since the resolution of the spectrometer used to collect these data was determined from measurements of the Fermi edge of a clean Ag specimen to be 0.40

TABLE III. A table of the differences in binding and kinetic energies, and in Auger parameters between the two identified Sb environments in Si, and their comparison with the bulk elemental material.

Binding- and kinetic-energy differences between Sb environments in eV			
	δ_1 bulk	δ_2 bulk	$\delta_2 - \delta_1$
ΔE_b	0.0	0.85	0.85
ΔE_k	-1.4	-1.4	0.0
$\Delta\alpha$	-1.4	-0.55	0.85
$\Delta\beta$			2.55

eV, it is clear that there is a substantial inhomogeneous broadening contribution to the measured peak widths. We attribute this additional broadening to a spread of environments associated with the main active and inactive sites, and to a local variation in band bending.

Although the photoemission results show that there are two Sb environments in the δ -doped layer, it is not possible to resolve the contributions from the two environments to either the 1G_4 component of the $L_3M_{4,5}M_{4,5}$ group or the $M_{4,5}N_{4,5}N_{4,5}$ Auger profiles of Sb. Our measurement of the profile of the $L_3M_{4,5}M_{4,5}; ^1G_4$ has been made at a significantly higher resolution than that measured earlier from elemental Sb,^{20,21} and this is reflected in the smaller linewidth of the measured Auger $L_3M_{4,5}M_{4,5}; ^1G_4$ spectrum. Consideration of the natural linewidth of this spectral feature together with the knowledge of the instrumental resolution enables us to put an upper limit of ~ 0.4 eV on any possible difference in the kinetic energy of the Auger spectra from the two sites. An analysis of the spectral profile of the $M_{4,5}N_{4,5}N_{4,5}$ transitions is consistent with this result, although the latter is only sufficient to put an upper limit of 0.8 eV on the possible separation of contributions from the two sites.

Recent work has shown that important insights into the differences in the local electronic structure of atomic environments can be obtained by a consideration of differences in Auger parameters.⁹⁻¹¹ The final-state Auger parameter α , defined by

$$\alpha = E_b + E_k, \quad (1)$$

where E_b is the binding energy of a core level measured by XPS, and E_k is the kinetic energy of a core-core-core Auger line, is particularly useful due to the cancellation of systematic differences in energy referencing of electron spectroscopy measurements on different specimens. The final-state Auger parameter α is thus a characteristic of the local electronic structure. In Table III we show the α parameters for bulk Sb and the δ_1 and δ_2 environments. Our inability to resolve two contributions to either the Sb $L_3M_{4,5}M_{4,5}; ^1G_4$ or $M_{4,5}N_{4,5}N_{4,5}$ Auger profiles means that there is an ambiguity in the values of α for the δ_1 and δ_2 sites, which from the high-resolution measurements on the $L_3M_{4,5}M_{4,5}; ^1G_4$ component is less than ± 0.2 eV. Even with this systematic uncertainty, neither the δ_1 nor the δ_2 site has an α equal to that of bulk Sb. However, the α for the δ_2 site is closest to that of the bulk, with $\Delta\alpha(\text{bulk} - \delta_2) = 1.7 \pm 0.2$ eV. The sensitivity of

the Auger parameter shifts to electronic structure is such that the differences in α of the δ_1 and δ_2 sites relative to bulk Sb are indicative of a significant reduction in final-state screening at both sites. Our expectation that at this concentration the donor (or active) sites will experience higher screening than the defect, cluster, or interstitial sites with their more localized valence wave functions leads us to associate the δ_2 site with the donors. The implication that any Sb clusters are less well screened than bulk Sb is not surprising if the possible sizes of the clusters are considered. From an analysis of the core-level photoemission data, we know there is no surface environment for Sb, and extensive structural studies of similar SPE-grown δ layers^{24,25} has revealed that Sb diffusion does not occur into the bulk of the Si crystal. This puts an upper limit on the diameter of an Sb cluster to be less than the depth of the δ layer (25 Å), which in turn limits the ratio of surface:bulk Sb atoms in the cluster to be at least 1:3. Allowing for a distribution in Sb cluster size (less than the maximum) can only increase the number of "surface" Sb atoms in the cluster relative to those in the "bulk." These clusters cannot therefore be regarded as "bulklike" Sb, and so the observed reduction in the final-state screening is reasonable.

It is possible to obtain a more detailed analysis of the differences in electronic structure between the two sites and between them and bulk Sb by extending the analysis to include a consideration of the initial-state Auger parameter β , and the analysis of the $\Delta\alpha$ and $\Delta\beta$ shifts in terms of a potential model. Such an analysis can give valuable insight into both ΔV , the environmental dependence of the atomic core potential, and ΔR , differences in final-state relaxation energies. By exploiting their different scaling with number of core holes, initial- and final-state effects may be separated using¹²

$$\Delta\beta = 2\Delta E_b(j) + \Delta E_b(i) + \Delta E_k(ijj) \sim 2\Delta V + 2\Delta\phi, \quad (2)$$

$$\Delta\alpha = 2\Delta E_b(j) - \Delta E_b(i) + \Delta E_k(ijj) \sim 2\Delta R, \quad (3)$$

where ϕ is a referencing potential. Ground-state potential shifts have long been interpreted using an electrostatic model which assumes that the contribution to the core potential due to the valence charge density, V^v is proportional to the local charge. The scaling constant k is of the order of the reciprocal atomic radius.¹³ Including the extra-atomic (Madelung) potential $M\Delta q$, we obtain

$$\Delta V = \Delta q(k - M). \quad (4)$$

Thomas and Weightman¹³ have shown that k can be determined using atomic structure calculations.

Recently an extended potential model has been developed¹⁴ which benefits from the simplicity of the potential model approach, while accounting for the dependence of k on core occupancy N , and valence charge q . This allows final-state effects to be treated using a Taylor-series expansion of the core potential.²⁶ The variation of atomic Dirac-Fock core eigenvalues with N and q is consistent with the parametrized form,

$$k(N, q) = a + bN + dq, \quad (5)$$

Potential shifts can then be expressed

$$\Delta V = (k_0 + bN - M)\Delta q + \frac{d}{2}(\Delta q)^2. \quad (6)$$

In the above expressions, the core occupancy is defined as the negative of the number of core holes, q the negative of the total number of valence electrons, and k_0 the value of k at the ground state ($N=0$, $q=q_0$). The coefficient b represents the contraction of the valence orbitals upon core ionization, while d represents the decrease in valence radius with increasing valence charge (i.e., with a reduced number of negatively charged electrons).

To model the extra-atomic screening of core holes, we use the excited-atom approach,^{26,27} which replaces a core-ionized site in the solid with a core-ionized atom to which dq/dN additional valence electrons have been added self-consistently. We obtain

$$\Delta\beta = \Delta \left\{ 2aq + dq^2 - \frac{2}{3} \frac{dq}{dN} \times \left[2b + d \frac{dq}{dN} \right] + 2V^{\text{ea}} \right\} + \Delta\phi, \quad (7)$$

$$\Delta\alpha = \Delta \left\{ qb \frac{dq}{dN} \left[a - 2b + d \left(q - \frac{dq}{dN} \right) \right] + \frac{dV^{\text{ea}}}{dN} \right\}. \quad (8)$$

We note that while the initial-state Auger parameter should be sensitive to the ground-state charge transfer, $\Delta\beta$ is not a reference-free quantity and usually contains a large experimental error due to surface dipole shifts. However, in the present case the contributions from the two distinct Sb sites in the Sb δ -doped Si specimen are measured in the same spectrum, and the referencing errors are implicitly removed ($\Delta\phi=0$). According to Eqs. (7) and (8), the chemical shifts $\Delta\alpha$ and $\Delta\beta$ are each determined by the elemental constants a , b , and d , and the values of q and dq/dN in the two environments. Potential model parameters for Sb have been computed using a Dirac-Fock code, as described previously.¹⁴ The values $a=15.25$ eV, $b=-1.75$ eV, and $d=1.55$ eV were obtained, corresponding to a ground-state k value of $k_0=7.5$ eV. If q and dq/dN are then known for some reference material, it is possible to determine solution curves ($q, dq/dN$) which reproduce experimental Auger parameter shifts for some unknown environment. We now use this approach to interpret the chemical shifts observed between δ_1 and δ_2 , and between these species and bulk Sb.

We assume that both sites are sufficiently localized in the δ -doped layer for V^{ea} in Eq. (7) to be zero, and that the clusters or interstitial defects are uncharged. As discussed earlier, we denote the Sb environment with the higher core-level photoelectron binding energy as δ_2 , and that with the lower binding energy as δ_1 , i.e., $\Delta E_b(\delta_2 - \delta_1) > 0$. While we are able to place an upper bound on the magnitude of the Auger shift $\Delta E_k(\delta_2 - \delta_1)$, we do not know its sign. In principle we must consider the two extreme cases in which $\Delta E_k(\delta_2 - \delta_1) = +0.4$ eV and $\Delta E_k(\delta_2 - \delta_1) = -0.4$ eV. For simplicity we start by taking $\Delta E_k = 0.0$ eV.

We now consider the simultaneous equations (7) and (8) for the shifts between bulk Sb and site δ_1 , with the knowledge that $q(\text{bulk}) = -5$ and $dq/dN(\text{bulk}) = 1$. As $\Delta\beta$ for this comparison is subject to an unknown referencing shift, the charge state cannot be reliably determined. However the dependence of $\Delta\alpha$ on $q(\delta_1)$ is very weak, and we obtain

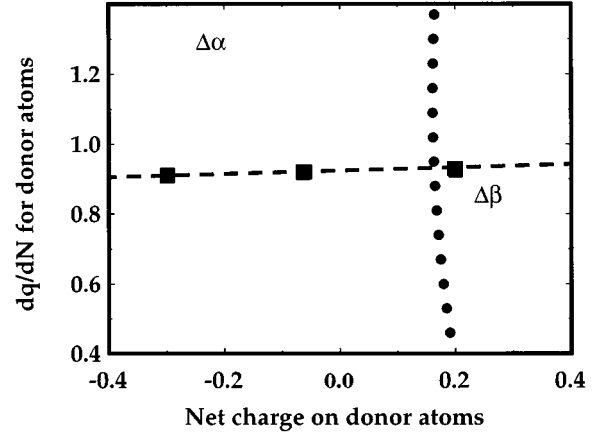


FIG. 4. A graph of the solution set for $q(\delta_2)$, $dq(\delta_2)/dN$ is plotted in the physically significant portion of parameter space. The solution curve determined from the expression for $\Delta\alpha$ allows only a narrow range of values for the screening efficiency dq/dN , while the $\Delta\beta$ solution curve specifies the ground-state charge. The intersection of the two solution curves indicates a donation of 0.16 electrons per active Sb atom.

$dq/dN(\delta_1) = 0.82$ for all physical values of $q(\delta_1)$. Similarly, for site δ_2 we obtain $dq/dN(\delta_2) = 0.93$. These results suggest that the core-hole screening environment of both components of the Sb δ layer in Si is poorer than that of elemental Sb, as one might expect.

We now examine the shifts between the two Sb environments (Table II), and find that $\Delta\beta(\delta_2 - \delta_1)$ is positive, consistent with δ_2 corresponding to the positively charged donors and δ_1 to neutral interstitial-defect-cluster sites. Conversely, if we associate δ_1 with the donors and δ_2 with the interstitial-defect-cluster sites, then this implies that donors are negatively charged, contrary to expectation for pentavalent Sb. This identification of the δ_2 component with the donor sites also makes sense of the difference in electron screening noted by the earlier analysis of the Auger parameter shifts $\Delta\alpha$, since for the donor sites (δ_2) the delocalized nature of the valence wave functions will give access to screening by the electron gas.

We can evaluate the magnitude of the donor charge by solving Eqs. (7) and (8) for δ_2 , assuming $q(\delta_1) = -5$ and $dq/dN(\delta_1) = 0.82$. The solution set $q(\delta_2)$, $dq(\delta_2)/dN$ is plotted in Fig. 4 in the physically significant portion of parameter space. It can be seen that the solution curve determined from the expression for $\Delta\alpha$ allows only a narrow range of values for the screening efficiency dq/dN , while the $\Delta\beta$ solution curve specifies the ground-state charge. The intersection of the two solution curves in Fig. 4 determines $q(\delta_2)$, $dq(\delta_2)/dN$ consistent with the experimental data. We conclude that our model indicates a donation of 0.16 electrons per active Sb atom. Returning now to the two extreme cases arising from the ambiguity in determining any shift in the Auger spectra from the two sites, we find a maximum charge estimate of 0.20 electrons per Sb and a minimum of 0.12 electrons per Sb. This is in close agreement with resistivity measurements made on similar samples (at 77 K), which were found to exhibit $\sim 20\%$ electronic activation of the dopant atoms.²⁸

CONCLUSIONS

We have shown that the creation of a highly concentrated layer of Sb dopant atoms in SPE-grown Si results in the formation of two main sites, the δ_1 and δ_2 , which can be identified by XPS. The $L_3M_{4,5}M_{4,5}$ and $M_{4,5}N_{4,5}N_{4,5}$ Auger spectra cannot be resolved into components arising from each site, and this puts an upper limit of 0.4 eV on the difference in the kinetic energies of the Auger spectra from each site. An analysis of the final-state Auger parameter shifts between the two sites and bulk Sb shows that core holes on each site are less well screened than in the pure element. A simultaneous analysis of shifts in the initial- and final-state Auger parameters of the two sites and bulk Sb shows that a consistent analysis of the data can be achieved provided that the δ_2 site is identified with positively charged donors, and the δ_1 site with neutral Sb which might arise from clusters, defects, or interstitial sites. The donors are found to contribute between 0.12 and 0.20 electrons per Sb atom, in agreement with results of transport measurements on similar specimens. The on-site screening of core holes on

the two sites, dq/dN , is found to be 0.82 and 0.93 for the δ_1 and δ_2 sites, respectively. This result is consistent with the expectation that the donor site will be better screened by access to the electron gas of donated electrons.

In addition to the results obtained for the Sb δ -doped Si(001) system, this study demonstrates that the analysis of electron spectroscopy measurements of Auger parameter shifts has considerable potential for yielding important information on the charge state and local screening of impurity systems relevant to research aimed at controlling semiconductor heterojunctions.

ACKNOWLEDGMENTS

The authors would like to acknowledge the help from A. W. Robinson and V. R. Dhanak in performing these measurements, T. P. Morrison and A. A. Cafolla in developing analysis software, and support from the Basic Research Action of ESPRIT (EASI;6878) and the HCMP network; PESSI, funded by the European Commission.

-
- ¹H. Jorke, *Surf. Sci.* **193**, 569 (1989).
²K. D. Hobart, D. J. Godbey, and P. E. Thompson, *Appl. Phys. Lett.* **61**, 76 (1992).
³E. V. Thomsen, O. Hansen, K. Harrekilde-Petersen, J. L. Hansen, S. Y. Shiryaev, and A. Nylandsted Larsen, *J. Vac. Sci. Technol. B* **12**, 3016 (1994).
⁴A. A. van Gorkum, K. Nakagawa, and Y. Shiraki, *Jpn. J. Appl. Phys.* **26**, L1933 (1987).
⁵H.-J. Gossmann, E. F. Schubert, D. J. Eaglesham, and M. Cerullo, *Appl. Phys. Lett.* **57**, 2440 (1990).
⁶C. van Opdorp, L. J. van Ijzendoorn, C. W. Fredriksz, and D. J. Gravesteijn, *J. Appl. Phys.* **72**, 4047 (1992).
⁷A. Casel, H. Kibbel, and F. Schäffler, *Thin Solid Films* **183**, 351 (1989).
⁸A. A. van Gorkum, K. Nakagawa, and Y. Shiraki, *J. Appl. Phys.* **65**, 2485 (1989).
⁹S. D. Waddington, P. Weightman, J. A. D. Matthew, and A. D. C. Grassie, *Phys. Rev. B* **39**, 10 239 (1989).
¹⁰A. Evans, A. D. Laine, P. Weightman, J. A. D. Matthew, D. A. Woolf, D. I. Westwood, and R. H. Williams, *Phys. Rev. B* **46**, 1513 (1992).
¹¹R. J. Cole, J. A. Evans, P. Weightman, J. A. D. Matthew, D. A. Woolf, and D. I. Westwood, *Phys. Rev. B* **49**, 7528 (1994).
¹²R. J. Cole and P. Weightman, *J. Phys. Condens. Matter* **6**, 5783 (1994).
¹³T. D. Thomas and P. Weightman, *Phys. Rev. B* **33**, 5406 (1986).
¹⁴R. J. Cole, D. A. C. Gregory, and P. Weightman, *Phys. Rev. B* **49**, 5657 (1994).
¹⁵A. A. van Gorkum, G. F. A. van de Walle, R. A. van de Heuvel, D. J. Gravesteijn, and C. W. Fredriksz, *Thin Solid Films* **184**, 207 (1990).
¹⁶P. Weightman, *Phys. Scr.* **T41**, 277 (1992).
¹⁷S. Doniach and M. Sunjic, *J. Phys. C* **3**, 285 (1970).
¹⁸M. Pessa, A. Vouristo, M. Vulli, S. Aksela, J. Väyrynen, T. Rantala, and H. Aksela, *Phys. Rev. B* **20**, 3115 (1979).
¹⁹M. O. Krause and J. H. Oliver, *J. Phys. Chem. Ref. Data* **8**, 329 (1979).
²⁰J.-M. Mariot and M. Ohno, *Phys. Rev. B* **34**, 2182 (1986).
²¹G. G. Kleiman, R. Landers, P. A. P. Nascente, and S. G. C. de Castro, *Phys. Rev. B* **46**, 1970 (1992).
²²S. J. Fukatsu, S. Kubo, Y. Shiraki, and R. Ito, *J. Cryst. Growth* **111**, 843 (1991).
²³E. I. Levin, M. E. Raikh, and B. I. Shklovskii, *Phys. Rev. B* **44**, 11 281 (1991).
²⁴W. F. J. Slijkerman, P. M. Zagwijn, J. F. van der Veen, A. A. van Gorkum, and G. F. A. van der Walle, *Appl. Phys. Lett.* **55**, 963 (1989).
²⁵W. F. J. Slijkerman, J. M. Gay, P. M. Zagwijn, J. F. van der Veen, J. E. Macdonald, A. A. Williams, D. J. Gravesteijn, and G. F. A. van der Walle, *J. Appl. Phys.* **68**, 5105 (1990).
²⁶A. R. Williams and N. D. Lang, *Phys. Rev. Lett.* **40**, 954 (1978).
²⁷L. Ley, S. P. Kowalczyk, F. R. McFeely, R. A. Pollack, and D. A. Shirley, *Phys. Rev. B* **8**, 2302 (1973).
²⁸D. J. Gravesteijn (unpublished).